Chemical Engineering Journal 331 (2018) 536–544

Contents lists available at ScienceDirect

Chemical Engineering Journal

journal homepage: www.elsevier.com/locate/cej

Use of a non-thermal plasma technique to increase the number of chlorine active sites on biochar for improved mercury removal

Tao Wang[a,*], Jun Liu[a], Yongsheng Zhang[a,*], Huicong Zhang[a], Wei-Yin Chen[b], Pauline Norris[c], Wei-Ping Pan[a,c]

[a] Key Laboratory of Condition Monitoring and Control for Power Plant Equipment, Ministry of Education, North China Electric Power University, Beijing 102206, China
[b] Department of Chemical Engineering, University of Mississippi, 134 Anderson Hall, University, MS 38677, USA
[c] Institute for Combustion Science and Environmental Technology, Western Kentucky University, Bowling Green, KY 42101, USA

GRAPHICAL ABSTRACT

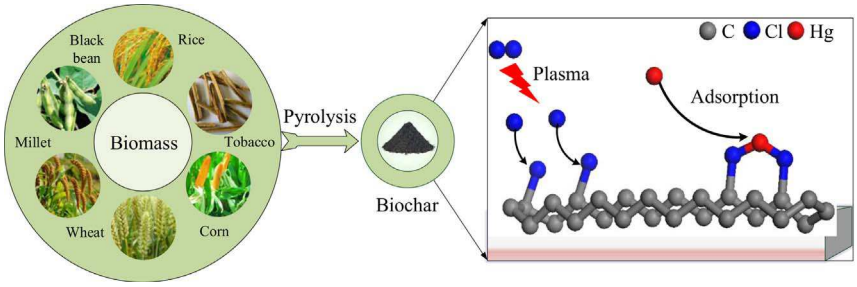

ARTICLE INFO

Keywords:
Non-thermal plasma
Biochar
Elemental mercury
Chlorine
Flue gas

ABSTRACT

Biochar, known as a byproduct of biomass pyrolysis, was prepared from rice straw (R6), tobacco straw (T6), corn straw (C6), wheat straw (W6), millet straw (M6), and black bean straw (B6) in high purity nitrogen at 600 °C. Chlorine (Cl) non-thermal plasma was used to increase Cl active sites on biochar to promote the mercury removal efficiency. The physio-chemical properties of biochar were characterized by proximate analysis, ultimate analysis, BET, SEM, TGA, FTIR, and XPS. Modification by chlorine plasma increased the Hg^0 removal efficiency of the biochar from around 8.0% to 80.0%. The Hg^0 adsorption capacity of T6 was 36 times higher after Cl_2 plasma modification. Plasma caused the biochar surface to become porous and promoted the thermal stability of the biochar. Sulfur (S) content remained in the range of 0.5–0.7%, elemental/organic sulfur and sulfide were converted to sulfate during plasma treatment. The relative intensity of the oxygen functional groups (C—O, C═O and C(O)—O—C) were enhanced, while the content of oxygen (O) in biochar decreased. The main reason for the improved mercury removal efficiency by modified biochars was attributed to the increased number of C—Cl groups on the surface of the biochars induced by Cl_2 plasma. The C—Cl groups functioned as activated sites and promoted the Hg^0 removal efficiency.

1. Introduction

Mercury has received more and more attention because it is a human health hazard and because it can bioaccumulate in the ecosystem. There are three main forms of mercury [1]: elemental mercury (Hg^0), particulate-bound mercury (Hg^p), and oxidized mercury (Hg^{2+}). Hg^0 is of high concern owing to its low reactivity, low melting point and low water solubility. Numerous methods have been

* Corresponding authors.
E-mail addresses: wangtao0420@163.com (T. Wang), yszhang@ncepu.edu.cn (Y. Zhang).

http://dx.doi.org/10.1016/j.cej.2017.09.017
Received 8 July 2017; Received in revised form 1 September 2017; Accepted 4 September 2017
Available online 07 September 2017
1385-8947/

developed to control Hg^0 emission including photochemical oxidation [2,3], sorbent adsorption [4–6], and non-thermal plasma [7–9]. Activated carbon (AC) sorbents have been used for capturing Hg^0 in coal-fired power plants [10], but its high cost limits full-scale applications. Biochar, made from pyrolyzed agricultural waste in an oxygen-free environment, is a byproduct of biomass pyrolysis. Biochar costs less and is relatively simple to prepare, so it an attractive alternative sorbent. Previous research indicates that the Hg^0 removal efficiency of raw biochar is only 1.2% [11]. The adsorption capacity of Hg^0 to commercial activated carbons is approximately 2–3 orders of magnitude stronger than unactivated biochar [12]. Therefore, many researchers aim to improve the adsorption capacity of biochar by physical or chemical modification techniques.

The physical modification technique mainly changes the pore structure such as specific surface area, pore volume and pore size of the biochar by heating [4,12,13], microwave [14,15], and ultrasonic [16]. Shu et al. [4] reported that steam heating activation increased the specific surface area and pore volume, enhancing mercury adsorption capacity from 5.07 to 8.76 μg/g. Li et al. [14] showed that the initial Hg^0 removal efficiency of biochar increased from 35.1% to 50.2% after microwave activation.

Chemical modification techniques mainly include acid [17–20], alkali [21,22], sulfur (S) [22,23], and halogen (Cl, Br, I) [24–27] modification. Chemical modification increases active functional groups on the surface of biochar, improving the chemical adsorption of mercury. It was reported that Hg^0 adsorption capacity reached 6067 μg/g in 700 h [18] and removal efficiency was more than 95% [19] using hydrochloric acid-modified biochar. Hg^0 adsorption capacity increased from 730 μg/g to 956 μg/g after NaOH activation [21]. Mercury removal efficiency of KOH and Na_2S modified biochar also increased by 32% and 77% [22], respectively. Tan et al. [20,26,27] also discussed the effect of H_2O_2, $ZnCl_2$, $FeCl_3$, NH_3, H_2O, and HNO_3 modification on Hg^0 adsorption by biochar. Li et al. [14] demonstrated that Hg^0 removal efficiency of chemically modified biochar was about 2–3 times higher than physically modified biochar. However, chemical modification is complex, time-consuming, and the added element could leach from the biochar and cause a pollution problem. The modification process will be more feasible if a simple, time-saving and efficient method is developed.

Non-thermal plasma produces energetic electrons, ions and active radicals that improve the pore structure of sorbent and increase the active functional groups on the surface of sorbent [28–31]. Zhang et al. [32,33] indicated that the removal efficiency of mercury with original AC was 56.3%. While the removal efficiency of mercury with air plasma-modified AC and Cl_2 plasma-modified AC was 80% and 96%, respectively. Pure N_2 plasma modification, however, decreased the mercury removal performance. Zhang et al. [34] found that the average Hg^0 removal efficiency of modified sorbent with O_2 plasma was about 2–3 times higher than that of raw sorbent. However, few studies have used non-thermal plasma techniques to increase the chlorine active sites on biochar to improve mercury removal.

In this paper, six raw materials, rice straw, tobacco straw, corn straw, wheat straw, millet straw, and black bean straw were pyrolyzed in high purity nitrogen to produce biochar. Dielectric barrier discharge (DBD) plasma was used to modify biochar in chlorine gas (Cl_2), and the effect of Cl_2 plasma modification on Hg^0 removal by different biochars were investigated. Proximate analysis, ultimate analysis, Brunauer–Emmett–Teller (BET), scanning electron microscope (SEM), thermogravimetric analysis (TGA), fourier transform infrared spectroscopy (FTIR), and X-ray photoelectron spectroscopy (XPS) were conducted to reveal possible Hg^0 adsorption properties and mechanisms using modified biochar.

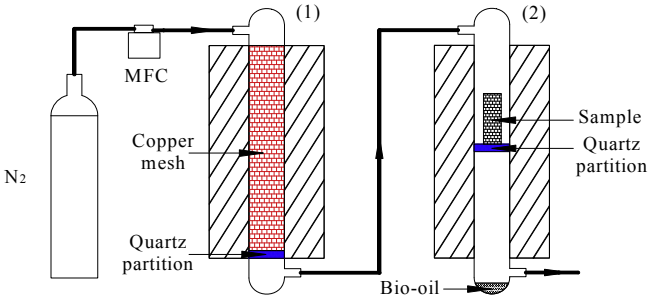

Fig. 1. Schematic diagram for preparation of biochar.

2. Materials and methods

2.1. Preparation of biochar

The raw materials for the biochar come from different regions in China. Corn straw, millet straw, wheat straw, and black bean straw were collected from the Shaanxi province. Rice straw was from the Anhui province and the tobacco straw came from the Henan province. The straws were washed by deionized water 3 times to remove impurities, and then dried at 110 °C for 24 h. The washed samples were ground using a ball mill and sieved between 100 and 200 mesh. The preparation process is shown in Fig. 1. Ten grams samples were wrapped in a copper mesh (200 mesh) and placed in the center of reactor 2 then heated by an electrical furnace. The length of the heating element was 50 cm, to minimize axial temperature differences in samples. In reactor 1, the copper mesh was used to remove the trace oxygen in the high purity nitrogen at 500 °C, ensuring the purity of the biochar [16]. The flow rate of N_2 was controlled at 300 mL/min by mass flow controllers (MFCs). Furnace 2 was set to 600 °C at 10 °C/min and held for 1 h, then naturally cooled down to room temperature in high purity nitrogen. After the pyrolysis process, the biochars of rice straw, tobacco straw, corn straw, wheat straw, millet straw, and black bean straw were denoted as R6, T6, C6, W6, M6, and B6, respectively.

2.2. Modification of biochar by plasma

As shown in Fig. 2, 0.3 g biochar was loaded in a DBD plasma reactor and that was sealed with high-vacuum silicon grease. One percent Cl_2 (N_2 as balance) was introduced into the reactor at 100 mL/min and the biochar was modified by Cl_2 plasma for 5 min. Nitrogen was introduced into reactor to purge the residual Cl_2 at 600 mL/min for 5 min after plasma modification. The modified biochars were named as R6Cl and T6Cl, C6Cl, W6Cl, M6Cl and B6Cl, respectively. The DBD reactor

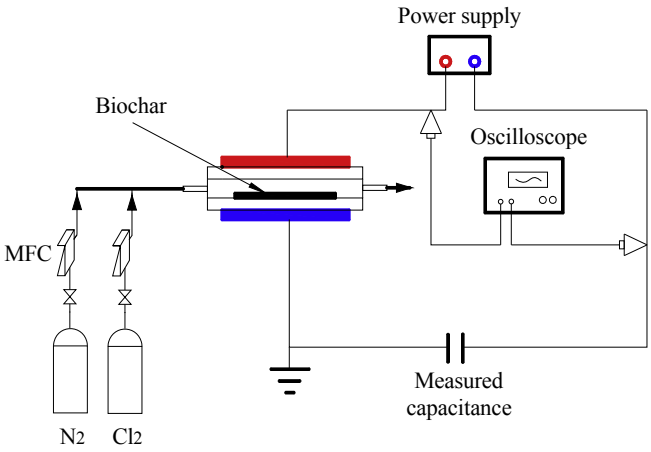

Fig. 2. Schematic of non-thermal plasma modification.

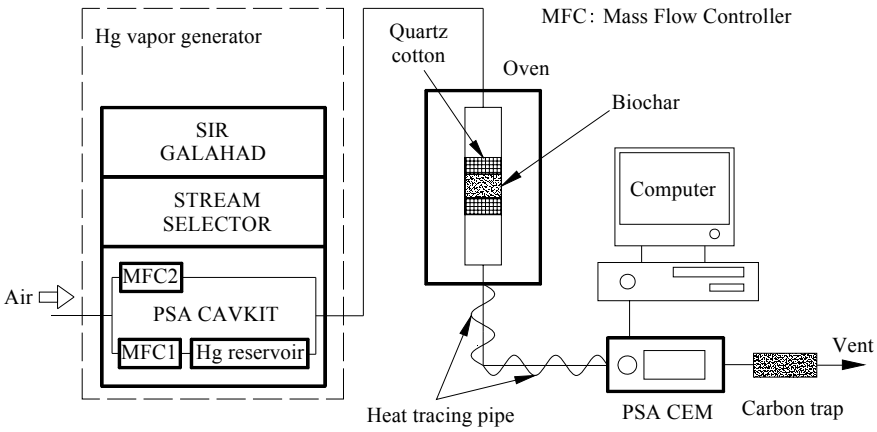

Fig. 3. Schematic of Hg^0 adsorption in a fixed-bed system.

consisted of two quartz plates with a thickness of 3 mm and a diameter of 70 mm. The electrodes were stainless steel with a diameter of 50 mm. The gas gap between the two quartz plates is 8 mm. The plasma was created by an alternating power current with a frequency of 10 kHz. The peak voltage was within 0–30 kV and the measured capacitance was 0.14 μF. An oscilloscope (Rigol DS1202CA) was used to determine the discharge power that was calculated from Lissajous figure. The discharge power of modification was 23 W.

2.3. Mercury adsorption experiment

The Hg^0 adsorption apparatus is shown in Fig. 3. It consists of a mercury vapor generating system, a fixed-bed adsorption system and a mercury Continuous Emission Monitor (CEM) system. The CEM system can measure the online elemental mercury concentration every 5 min. Elemental mercury vapor was supplied using the mercury source-PSA 10.536 Cavkit at a fixed temperature of 40 °C. Compressed air with a pressure of 0.2 Mpa was used as the carrier gas to transport Hg^0. A mass flow controller (MFC1) in the PAS Cavkit was used to transport Hg^0 vapor from the Hg reservoir, and the MFC2 regulated the dilution air. Total gas flow into the adsorption system was controlled at 2 L/min and the initial concentration of Hg^0 was set at 20 μg/m^3. A fixed-bed reactor was placed in a temperature-controlled oven. The temperature inside the oven was fixed at 150 °C. The fixed-bed reactor was a quartz tube with a length of 250 mm and an inner diameter of 6 mm. Approximately 0.05 g of sorbent was packed into the reactor and quartz cotton was used to keep the sorbent stationary. Heat tracing pipe, set at 140 °C, was used to prevent the Hg^0 from condensing. The outlet concentration of Hg^0 was continuously measured by the CEM system. The Hg^0 removal efficiency (η) was calculated by Eq. (1):

$$\eta = \frac{C_{in} - C_{out}}{C_{in}} \times 100\% \quad (1)$$

C_{in} and C_{out} are Hg^0 concentrations at the inlet and outlet of the adsorption system, respectively.

The adsorption capacity per unit quality of sorbent was calculated by Eq. (2):

$$q_t = \frac{Q}{m}\int_0^t (C_{in,0} - C_{out,t})dt \quad (2)$$

where q_t is adsorption capacity per unit quality of sorbent at t min (μg/g), Q is flow rate of gas (L/min), m is the mass of the sorbent (g), $C_{in,0}$ is the inlet Hg^0 concentration (μg/m^3), and $C_{out,t}$ is outlet Hg^0 concentration at t min (μg/m^3).

2.4. Biochar characterization

Carbon (C), hydrogen (H), nitrogen (N), and sulfur (S) content was measured using an EA3000 elemental analyzer. Moisture, ash and volatile matter content was measured using a LECO TGA701S4C. Analyses were completed in triplicate and the averages of the results were used. Biochars were analyzed using a Hitachi S4800 Scanning electron microscope (SEM). The thermal stability of the biochars was analyzed using a thermogravimetric analyzer (TAQ600). Ten milligrams of sample were used in the pyrolysis process, and then the samples were heated to 800 °C at 20 °C/min in high purity N_2. The specific surface area was measured using a nitrogen adsorption/desorption method at −196 °C on a Quantachrome Autosorb-iq-MP. The surface functional groups of the biochars were identified using Fourier transform infrared (FTIR) spectroscopy (PerkinElmer). Approximately 0.5 mg of biochar was mixed with 100 mg of KBr to make sample discs. The instrument was operated using a scan range of 4000–400 cm^{-1}. A PHI quantera SXM X-ray photoelectron spectroscopy (XPS) system was used to analyze the elemental states of C, O and Cl on the surface of the biochars.

3. Results and discussion

3.1. Mercury adsorption performance of raw biochars

A fixed bed system, shown in Fig. 4, was used to determine the Hg^0 removal efficiency and adsorption capacity of the six biochars. The Hg^0 removal efficiencies of the original biochars were less than 10.0%, exhibiting similar and poor Hg^0 adsorption performance. Initial removal efficiencies for R6 and T6 were 8.2%, but after 90 min, efficiencies decreased rapidly to 0% and 2.1% for R6 and T6, respectively. Adsorption capacities after 90 min were 16.1, 7.3, 3.2, 1.2, 0.9, and 0.3 μg/g for T6, R6, B6, W6, C6, and M6, respectively.

3.2. Effect of Cl_2 plasma modification on Hg^0 adsorption performance

As shown in Fig. 5, Cl_2 plasma modification has a positive influence on the Hg^0 removal efficiency of the six biochars. The initial Hg^0 removal efficiencies of R6Cl, T6Cl, C6Cl, W6Cl, M6Cl, and B6Cl were 83.9%, 84.2%, 42.7%, 52.7%, 81.1% and 5.3%, respectively. Modified tobacco biochar (T6Cl) had the best Hg^0 adsorption performance. The initial Hg^0 removal efficiency of T6Cl was almost 10 times higher than that of tobacco biochar without plasma modification (T6). After 90 min, the Hg^0 removal efficiency of T6Cl was still 55.8%. The T6Cl biochar had an adsorption capacity of 583.0 μg/g. R6Cl and M6Cl had similar adsorption capacities at 445.1 and 444.3 μg/g, respectively. The adsorption capacity of T6 was 36 times higher after Cl_2 plasma modification. The adsorption capacity of modified wheat (W6Cl) and corn (C6Cl) biochar increased to 217.6 and 150.8 μg/g, respectively. The Cl_2 plasma modification did not greatly improve the Hg^0 adsorption capacity of the black bean biochar (B6). The adsorption capacity only increased from 3.2 μg/g to12.6 μg/g after modification.

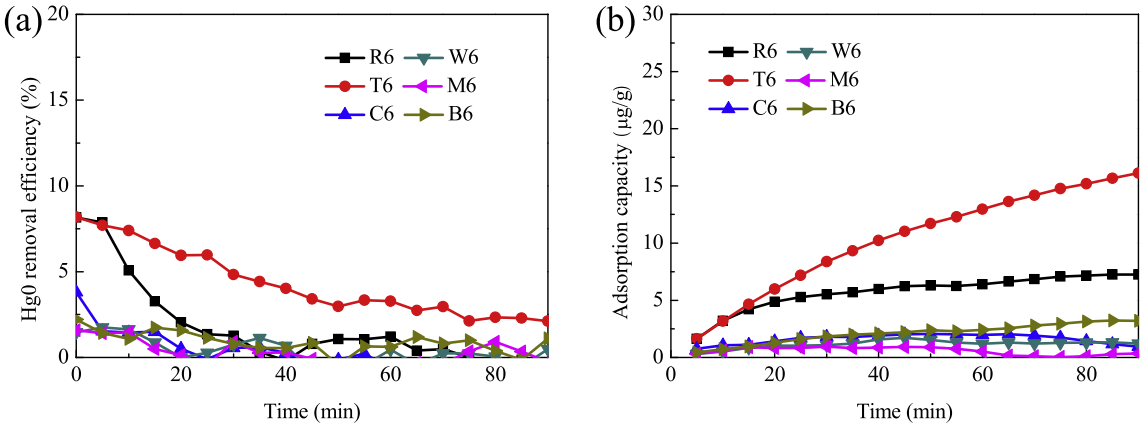

Fig. 4. Hg^0 removal efficiency and adsorption capacity of raw biochars.

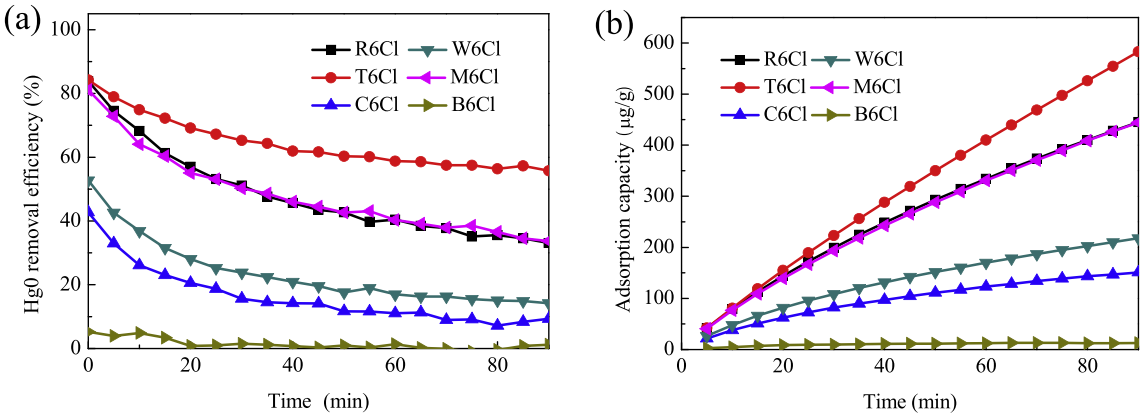

Fig. 5. Hg^0 removal efficiency and adsorption capacity of modified biochars.

Table 1
Properties of raw and modified biochars.

Sample	Proximate analysis (wt%)				Ultimate analysis (wt%)					S_{BET} (m^2/g)
	Moisture	Volatile matter	Ash	Fixed carbon	C	N	H	S	O[a]	
R6	4.7	9.3	40.2	45.8	47.8	0.6	0.6	0.5	10.3	17.4
T6	5.7	15.8	39.8	38.7	42.3	1.5	0.9	0.5	15.0	8.2
C6	5.8	12.9	22.6	58.7	47.9	2.2	1.0	0.7	25.6	10.9
W6	6.0	12.4	22.7	58.9	65.3	0.4	0.9	0.7	10.0	15.9
M6	5.0	12.8	32.9	49.3	56.8	0.9	1.2	0.6	7.6	63.8
B6	4.6	18.5	28.5	48.4	59.5	2.1	0.9	0.6	8.4	6.3
R6Cl	4.9	9.3	39.4	46.4	55.6	0.7	1.0	0.6	2.7	33.5
T6Cl	7.2	14.9	39.9	38.0	43.5	1.3	0.8	0.7	13.8	6.2
C6Cl	6.2	11.8	22.8	59.2	63.1	2.2	0.7	0.7	10.5	26.6
W6Cl	6.3	11.2	22.5	60.0	67.0	< 0.1	0.5	0.7	9.3	21.9
M6Cl	6.1	11.7	32.4	49.8	64.2	0.5	0.8	0.7	1.4	31.9
B6Cl	4.9	18.3	27.8	49.0	61.1	1.3	1.2	0.7	7.9	6.1

[a] O = 100 − (C + N + H + S + Ash).

3.3. Microstructure and composition of biochar

Table 1 shows the proximate analysis, ultimate analysis, and surface area of the six raw and modified biochars. The results show that the six raw biochars have similar basic properties. The carbon content of the six raw biochars was in the range of 42.3–65.3 wt%. Biochars R6 and T6 had lower carbon percentages (47.8% and 42.3%) and higher ash percentages (39.8% and 40.2%). Minerals, such as calcium and iron, in the ash can act as a catalyst to promote the oxidation of elemental mercury to oxidized mercury [35,36]. This may explain why tobacco and rice had the best mercury capturing capability. The B6 and T6 volatile matter percentages were 18.5% and 15.8%, respectively. The sulfur percentages of the six raw biochars were in the range of 0.5–0.7%, with C6 and W6 having the highest sulfur content. The C6 biochar had the highest oxygen content, 25.6%. The R6 and T6 biochars also had relatively high oxygen percentages. The surface area of all the raw samples ranged from 6.3 to 63.8 m^2/g. The T6 biochar had a poor surface area of 8.2 m^2/g. The Cl_2 plasma modification increased the carbon content of the biochars. Increased carbon content will improve the mercury adsorption capacity of the modified biochar. The oxygen content in M6Cl, C6Cl, W6Cl, R6Cl, B6Cl, and T6Cl decreased by 6.2%, 15.1%, 0.7%, 7.6%, 0.5%, and 1.2%, respectively. This is mainly due to the increase in carbon content in the modified biochar because the oxygen content is calculated by difference.

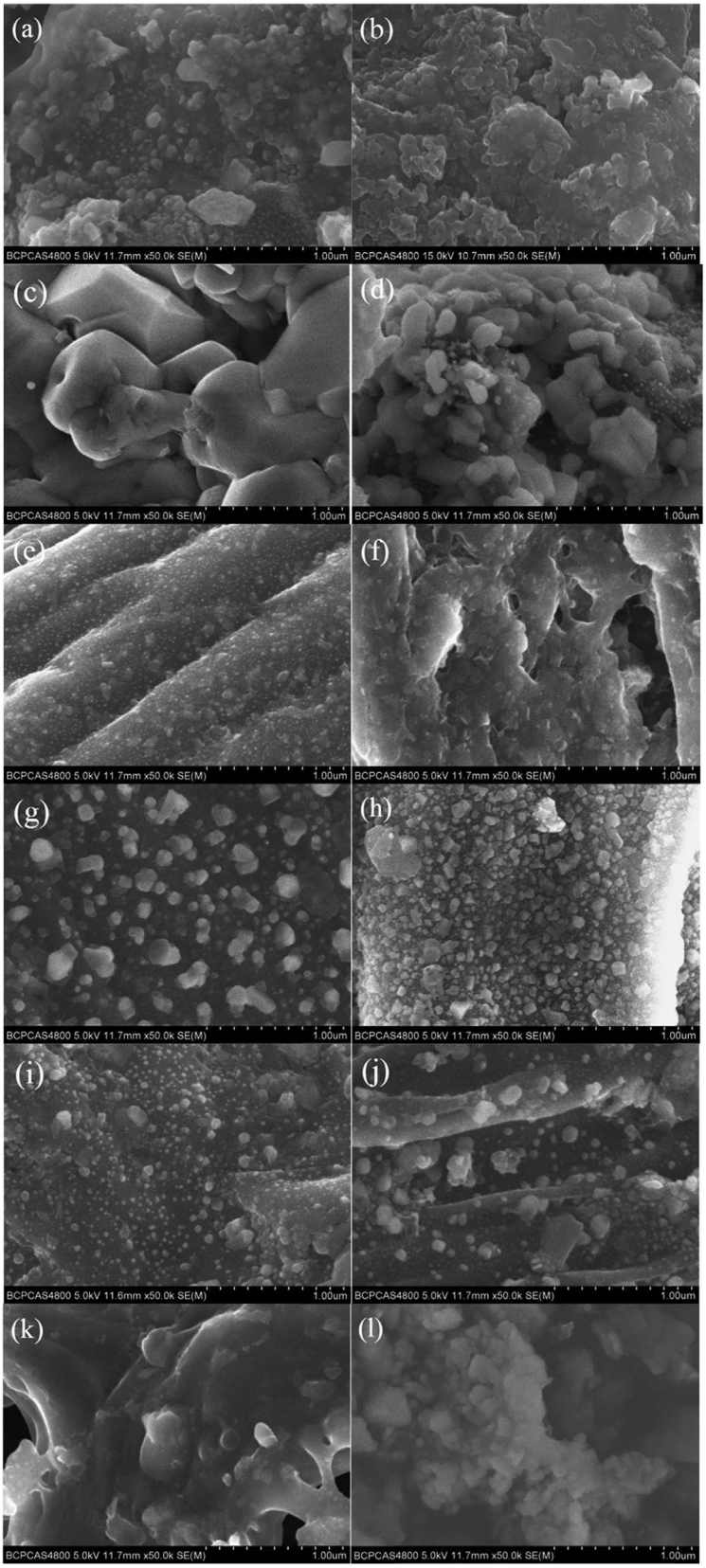

Fig. 6. SEM images of R6 (a); R6Cl (b); T6 (c); T6Cl (d); C6 (e); C6Cl (f); W6 (g); W6Cl (h); M6 (i); M6Cl (j); B6 (k); B6Cl (l).

The effect of plasma modification on the specific surface area of the six biochars was different. Plasma increased the specific surface area of R6, C6, and W6, and decreased the surface area of T6, M6 and B6. The Hg^0 adsorption capacity of T6Cl and M6Cl increased. Therefore, physical adsorption was not a key factor in Hg^0 removal. The influence of plasma on surface morphologies of six biochars are shown in Fig. 6(a)-(l). The surface textures of biochars were dense, undulating, compact and irregular due to the devolatilization. The surface texture of modified biochars were more porous and loose and the particles size on modified biochars were divided into small pieces due to plasma etching

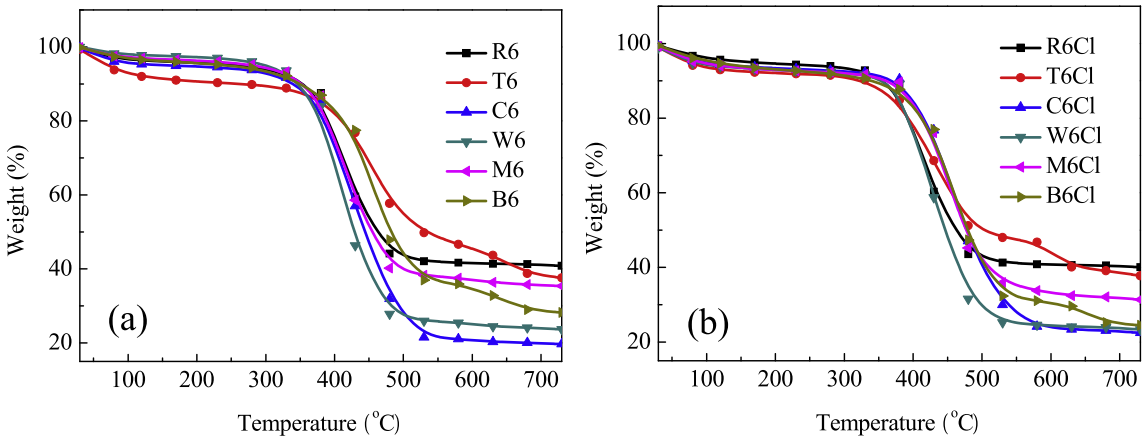

Fig. 7. TGA curves of raw and modified biochars.

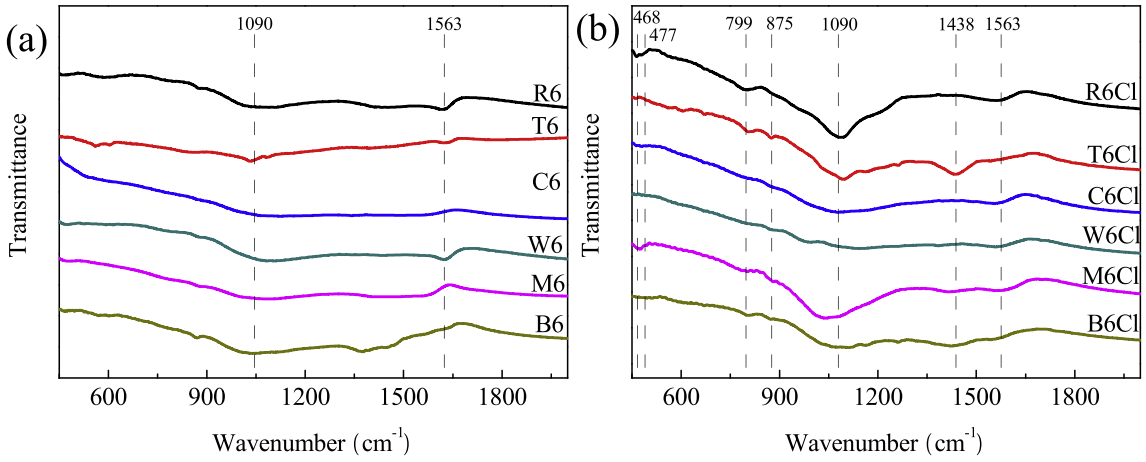

Fig. 8. The FTIR spectra of biochars.

effects. This was ascribed to the destruction of biochar by energetic electrons and active free radicals in the plasma system.

3.4. Effect of plasma on thermal properties of biochars

Thermogravimetric analysis in air was used to evaluate the thermal properties of raw and modified biochars, as shown in Fig. 7(a)-(b). Two weight losses were observed for both raw and modified biochars. The first mass loss is attributed to moisture loss and occurs between 30 and 150 °C. The biggest weight loss is attributed to the combustion of fixed carbon at 300–550 °C. The combustion temperature for modified biochars increased to 350–600 °C. The analysis indicated the stability of modified biochars increased by about 50 °C compared with raw biochars, and that modified biochars can be safely used below 350 °C. Samples R6, T6, C6, W6, M6, and B6 had residual weights of 40.9%, 37.6%, 19.7%, 23.7%, 35.4% and 28.2%, respectively. The weight remaining at 730 °C was attributed to the ash, which is consistent with the proximate analysis data in Table 1.

3.5. FTIR analysis

Fig. 8 shows the FTIR spectra of six biochars before and after modification. The wide adsorption peak at about 1438 and 1563 cm^{-1} represent the C=O stretching, which is attributed to various oxygen functional groups, such as ester, carboxyl and anhydride. The peak at around 1090 cm^{-1} is attributed to C—O bending. The adsorption peaks at about 875 cm^{-1} in the T6Cl and M6Cl samples are attributed to C—N. This could be because N_2 was the balance gas. The N_2 dissociated into N atoms in the plasma system and then N atoms attached to the surface of the biochar to form C—N. The peaks at 799, 477 and 468 cm^{-1} in the FTIR spectra of samples R6Cl, T6Cl and M6Cl represent the stretching vibration of C—Cl [37,38]. Shu et al. [4] indicated that the absorption peaks of Cl—C—Cl groups also appear at 1090 cm^{-1}, which overlap with the C—O peak. The intensity of the peak at 1090 cm^{-1} was larger for R6Cl, T6Cl and M6Cl. It was concluded that the Cl_2 plasma increased the number of C—Cl groups on the biochar surface, especially for R6Cl, T6Cl, and M6Cl. The data is consistent with the results of Hg^0 removal by modified biochars. R6Cl, T6Cl, and M6Cl have the best adsorptive activity for mercury of the six sorbents.

3.6. Modification and adsorption mechanism via XPS analysis

Samples were analyzed by XPS to explore the mechanism of Hg^0 adsorption and determine the chemical states present in biochar. The XPS spectra of R6, T6, R6Cl, T6Cl, used R6Cl, and used T6Cl samples are shown in Fig. 9. The XPS spectra contained C_{1s}, Cl_{2p} and S_{2p} peaks. The relative intensity of the C, O, and Cl functional groups were summarized in Table 2. As shown in Fig. 9(a) and (b), the C_{1s} spectra of R6, T6, R6Cl, and T6Cl can be divided into four peaks. The low peak in the range of 283.9–284.0 eV corresponding to C—C, the binding energy peak at 285.2 eV corresponding to C—O, and the peaks located at 286.9–287.0 eV and 288.6–288.7 eV corresponding to C=O and C(O)—O—C, respectively. The C—C group intensity of R6 and T6 was 83.8% and 88.7%, which decreased to 74.4% and 79.2% after Cl_2 plasma modification, respectively. However, the plasma treatment enhanced the relative intensity of the oxygen functional groups like C—O (ester,

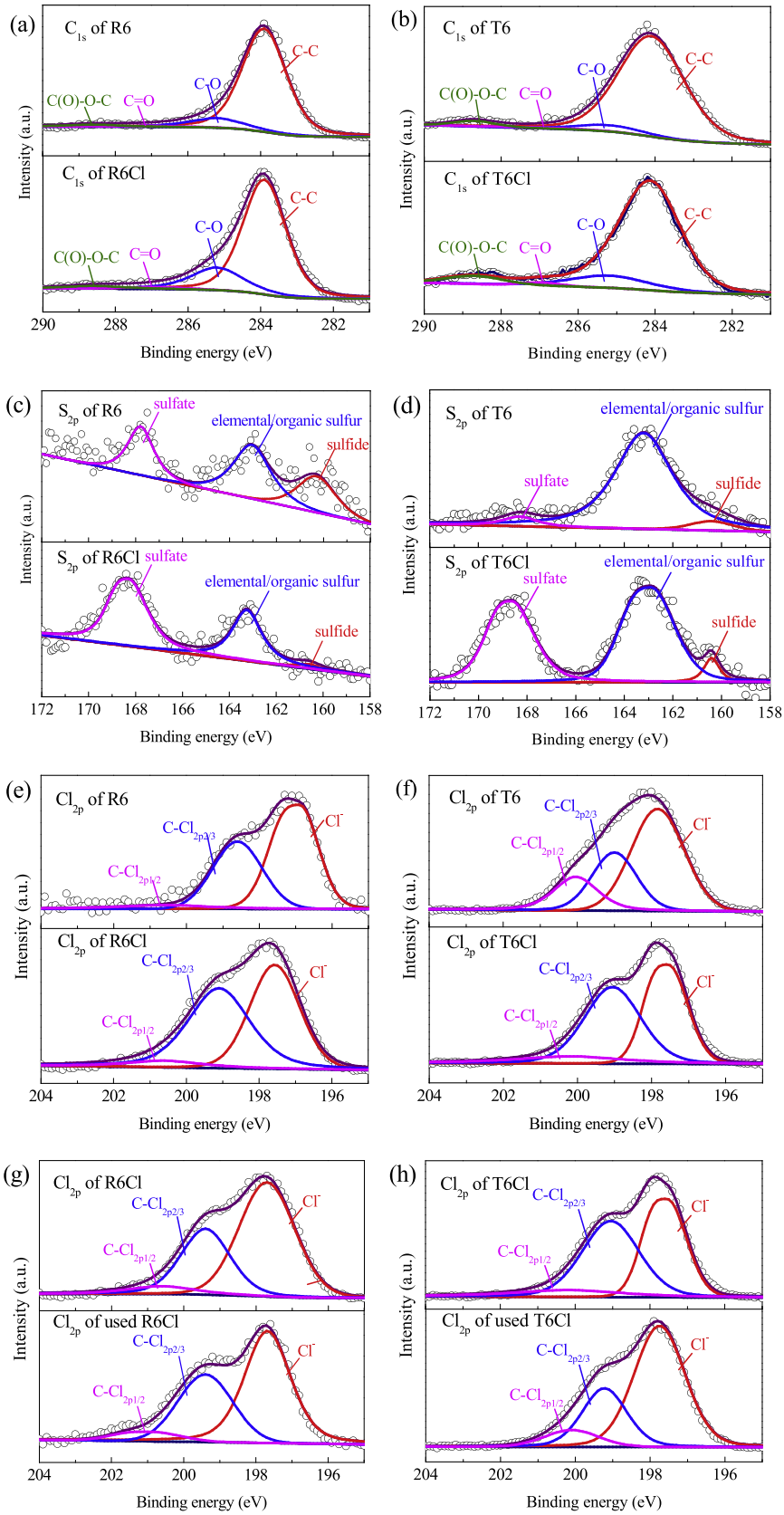

Fig. 9. XPS spectra of C_{1s}, S_{2p} and Cl_{2p} for biochars.

phenol, etc.), C=O (carbonyl, ester, carboxylic, etc.), and C(O)−O−C (ester groups). Zhang et al. [32–34] indicated that increasing chemical adsorption active sites of sorbent were more effective than improving the physical structure for Hg^0 adsorption. They also pointed out that C=O and C(O)−O−C act as the decisive chemisorption sites in the Hg^0 absorption process. The C=O and C(O)−O−C groups of R6 were 1.9% and 2.9%, which increased to 2.3% and 3.2%, respectively, after chemical modification. After plasma treatment, carbonyl and ester groups

Table 2
Functional groups determined from XPS spectra.

Functional groups	Binding energy (eV)	Relative intensity (%)					
		R6	R6Cl	Used R6Cl	T6	T6Cl	Used T6Cl
C—C	283.9–284.0	83.8	74.4	–	88.9	79.2	–
C—O	285.2	11.4	20.1	–	6.0	13.1	–
C═O	286.9–287.0	1.9	2.3	–	1.5	1.7	–
C(O)—O—C	288.6–288.7	2.9	3.2	–	3.6	6.0	–
Sulfide	160.3–160.6	28.6	2.7	–	5.6	4.8	–
Elemental/ organic sulfur	162.9–163.3	43.9	36.7	–	88.6	53.4	–
Sulfate	167.8–168.7	27.5	60.6	–	5.8	41.8	–
Cl^-	196.9–197.8	60.9	45.1	57.9	54.5	44.4	63.6
C—$Cl_{2p2/3}$	198.6–199.4	34.1	48.9	35.5	27.6	45.3	27.5
C—$Cl_{2p1/2}$	200.2–200.9	5.0	6.0	6.6	17.9	10.3	8.9

in T6 also increased from 1.5% and 3.6% to 1.7% and 6.0%, respectively. Lota et al. [39] reported that the intensity of C—O, C═O C(O)—O—C groups was increased by argon plasma. However, XPS spectra also show that plasma treatment decreased the total oxygen content of R6 and T6 from 25.7% and 28.1% to 22.3% and 26.6%, respectively. These results were consistent with the ultimate analysis, especially the decrease in the oxygen content in R6 from 10.3% to 2.7%, as shown in Table 1. This indicates that the activity of oxygen functional groups on Hg^0 removal by modified biochar was slight and can even be ignored.

Sulfur groups have been shown to promote the removal of Hg^0. The effect of Cl_2 plasma on S_{2p} is shown in Fig. 9(c) and (d). The peak at 160.3–160.6 eV corresponds to sulfide, the peak at 162.9–163.3 eV corresponds to elemental/organic sulfur, and the peak centered at 167.8–168.7 eV corresponds to sulfate. As shown in Table 2, elemental/organic sulfur was the main component of intrinsic sulfur for raw biochar, accounting for 43.9% and 88.6% for R6 and T6, respectively. After Cl_2 plasma modification, the content of elemental/organic sulfur and sulfide decreased, while the sulfate content of R6 Cl and T6 Cl increased to 60.6% and 41.8%, respectively. The sulfide groups could be oxidized to elemental sulfur, and then the active sites could be oxidizing Hg^0 into HgS [14,40]. Both elemental sulfur and sulfide served as active sites in the adsorption process in which the Hg^0 was oxidized to HgS by S. However, Cl_2 plasma decreased the content of the elemental sulfur and sulfide. The enhancement of Hg^0 removal by Cl_2 plasma activated biochars was not related to sulfur groups.

The study aims to generate Cl functional groups on the surface of biochars by using Cl_2 plasma. Attached Cl is an important factor for Hg^0 adsorption. To better understand the mechanism of modification by Cl_2 plasma, Cl_{2p} peaks from XPS spectra were used to discuss the evolution of Cl functional groups on the surface of R6 and T6 before and after Cl_2 plasma modification in Fig. 9(e) and (f). The results show that Cl content on the surface of R6 and T6 were 1.5% and 7.8%, which increased to 6.3% and 10.5% after plasma modification, respectively. Cl_{2p} peaks were deconvoluted into three components as shown in XPS spectra. The peak at 196.9–197.8 eV was due to ionic chlorine (Cl^-), and the other two peaks located at 198.6–199.4 eV and 200.2–200.9 eV corresponded to the C—Cl groups at $Cl_{2p2/3}$ and $Cl_{2p1/2}$. As shown in Table 2, the relative intensity of Cl^- for R6Cl and T6Cl decreased to 45.1% and 44.4%, while that of total C—Cl of R6Cl and T6Cl increased to 54.9% and 55.6%. This indicated that Cl^- represented the main part of R6 and T6, while C—Cl groups dominated on the surface of R6Cl and T6Cl. Therefore, Cl_2 plasma increased the number of Cl groups on the surface of biochars. The numbers of C—Cl groups in the R6Cl and T6Cl samples were 1.4 and 1.2 times higher than the R6 and T6 samples, respectively. After the Hg^0 adsorption process, the C—Cl group percentages in the used R6Cl and T6Cl biochars decreased to 42.1% and 36.4%, respectively, as shown in Fig. 9(g) and (h). The relative intensity of Cl^- in used R6Cl and T6Cl biochars increased to 57.9% and 63.6%, respectively. This implies that the C—Cl groups changed into Cl^- during the adsorption process. The C—Cl groups serve as activated sites and promote chemical adsorption, which oxidizes the Hg^0 into Hg^{2+} and then transfers to Cl^- during Hg^0 absorption [41,42]. One possible Hg^0 adsorption mechanism for Cl_2 plasma modified biochars can be ascribed as follows [14,33,43–45]:

$$Cl_2 + plasma \rightarrow 2Cl$$

$$C+ Cl \rightarrow C{-}Cl(ad)$$

$$Hg^0(g) + biochar \rightarrow Hg^0(ad)$$

$$Hg^0(ad) + 2C{-}Cl(ad) \rightarrow 2\ C+ HgCl_2(ad)$$

$$Hg^0(ad) + C{-}Cl(ad) \rightarrow C+ HgCl(ad)$$

$$HgCl(ad) + C{-}Cl(ad) \rightarrow C+ HgCl_2(ad)$$

In the plasma system, active electrons collided with chlorine molecules to produce Cl active radicals, and then attached on the biochar to form C—Cl groups. The Hg^0 transferred from the gas phase to the biochar surface and physically adsorbed onto the biochar. The adsorbed Hg^0 reacted with the C—Cl groups to form $HgCl_2$.

4. Conclusion

In this study, biochar pyrolysed from six straws were used to investigate Hg^0 adsorption. A novel modified method was proposed to improve Cl active sites on biochar by non-thermal plasma for Hg^0 removal. The Hg^0 removal efficiency was less than 10.0% by raw biochars, but increased to over 80.0% after modification by Cl_2 plasma. The Hg^0 adsorption capacity of T6Cl was almost 36 times higher than that of T6. The surface properties of biochars were analyzed by proximate analysis, ultimate analysis, BET, SEM, TGA, FTIR, and XPS. The results showed that carbon content increased, while the oxygen content decreased following plasma modification. Plasma increased the specific surface area of R6, C6 and W6, but decreased that of T6, M6 and B6. The biochar surface became porous and divided into small pieces by plasma etching. The combustion temperature of modified biochars increased about 50 °C compared with raw biochars. The relative intensity of the oxygen functional groups (C—O, C═O, and C(O)—O—C) were enhanced, and elemental/organic sulfur and sulfide transferred to sulfate during plasma treatment. The stretching vibration of C—Cl groups were obvious on the spectrums of R6Cl, T6Cl, and M6Cl. The numbers of C—Cl groups for samples R6Cl and T6Cl were 1.4 and 1.2 times higher, respectively, than the corresponding R6 and T6 samples. After the Hg^0 adsorption process, the C—Cl group percentages in the used R6Cl and T6Cl biochars decreased to 42.1% and 36.4%, respectively. It can be concluded that Cl_2 plasma modification increases the amount of C—Cl groups on the biochar surface, and that those C—Cl groups serve as activated sites that increase the Hg^0 removal efficiency.

Acknowledgements

This work was supported by National Natural Science Foundation of China (51706069) and the Fundamental Research Funds for the Central Universities (2017JQ002). Wei-Yin Chen's work on biochar activation is supported by the National Science Foundation Award of America (1632899).

References

[1] L. Zhong, W. Li, Y. Zhang, P. Norris, Y. Cao, W.P. Pan, Kinetic studies of mercury adsorption in activated carbon modified by iodine steam vapor deposition method, Fuel 188 (2017) 343–351.
[2] Y. Liu, J. Zhang, J. Pan, Photochemical oxidation removal of Hg^0 from flue gas containing SO_2/NO by an ultraviolet irradiation/hydrogen peroxide (UV/H_2O_2) process, Energy Fuels 28 (2014) 2135–2143.
[3] C.R. Mclarnon, E.J. Granite, H.W. Pennline, The PCO process for photochemical

removal of mercury from flue gas, Fuel Process. Technol. 87 (2005) 85–89.
[4] T. Shu, P. Lu, N. He, Mercury adsorption of modified mulberry twig chars in a simulated flue gas, Bioresour. Technol. 136 (2013) 182–187.
[5] S. Wang, Y. Zhang, Y. Gu, J. Wang, Z. Liu, Y. Zhang, Y. Cao, C.E. Romero, W.P. Pan, Using modified fly ash for mercury emissions control for coal-fired power plant applications in China, Fuel 181 (2016) 1230–1237.
[6] Y. Zhang, W. Duan, Z. Liu, Y. Cao, Effects of modified fly ash on mercury adsorption ability in an entrained-flow reactor, Fuel 128 (2014) 274–280.
[7] Q. Niu, J. Luo, S. Sun, Q. Chen, J. Lu, Effects of flue gas components on the oxidation of gaseous Hg^0 by dielectric barrier discharge plasma, Fuel 150 (2015) 619–624.
[8] Z.H. Wang, S.D. Jiang, Y.Q. Zhu, J.S. Zhou, J.H. Zhou, Z.S. Li, K.F. Cen, Investigation on elemental mercury oxidation mechanism by non-thermal plasma treatment, Fuel Process. Technol. 91 (2010) 1395–1400.
[9] Y. Zhang, Y. Zhang, T. Wang, J.W. Lin, C.E. Romero, W.P. Pan, Oxidation of elemental mercury with non-thermal plasma coupled with a wet process, Fuel 197 (2017) 320–325.
[10] Y. Liu, Y.G. Adewuyi, A review on removal of elemental mercury from flue gas using advanced oxidation process: chemistry and process, Chem. Eng. Res. Des. 112 (2016) 199–250.
[11] G. Li, B. Shen, F. Li, L. Tian, S. Singh, F. Wang, Elemental mercury removal using biochar pyrolyzed from municipal solid waste, Fuel Process. Technol. 133 (2015) 43–50.
[12] J.L. Gomezeyles, C. Yupanqui, B. Beckingham, G. Riedel, C. Gilmour, U. Ghosh, Evaluation of biochars and activated carbons for in situ remediation of sediments impacted with organics, mercury, and methylmercury, Environ. Sci. Technol. 47 (2013) 13721–13729.
[13] G.G. Choi, S.H. Jung, S.J. Oh, J.S. Kim, Total utilization of waste tire rubber through pyrolysis to obtain oils and CO_2 activation of pyrolysis char, Fuel Process. Technol. 123 (2014) 57–64.
[14] G. Li, S. Wang, F. Wang, Q. Wu, Y. Tang, B. Shen, Role of inherent active constituents on mercury adsorption capacity of chars from four solid wastes, Chem. Eng. J. 307 (2016) 544–552.
[15] K. Yang, J. Peng, C. Srinivasakannan, L. Zhang, H. Xia, X. Duan, Preparation of high surface area activated carbon from coconut shells using microwave heating, Bioresour. Technol. 101 (2010) 6163–6169.
[16] W.Y. Chen, D.L. Mattern, E. Okinedo, J.C. Senter, A.A. Mattei, C.W. Redwine, Photochemical and acoustic interactions of biochar with CO_2, and H_2O: applications in power generation and CO_2 capture, AIChE J. 60 (2014) 1054–1065.
[17] T. Bohli, A. Ouederni, Improvement of oxygen-containing functional groups on olive stones activated carbon by ozone and nitric acid for heavy metals removal from aqueous phase, Environ. Sci. Pollut. Res. 23 (2016) 1–10.
[18] K. Johari, N. Saman, S.T. Song, S.C. Cheu, H. Kong, H. Mat, Development of coconut pith chars towards high elemental mercury adsorption performance-effect of pyrolysis temperatures, Chemosphere 156 (2016) 56–68.
[19] K.T. Klasson, L.L.B. Jr, M. Uchimiya, I.M. Lima, Influence of biochar pyrolysis temperature and post-treatment on the uptake of mercury from flue gas, Fuel Process. Technol. 123 (2014) 27–33.
[20] Z. Tan, J. Qiu, H. Zeng, H. Liu, J. Xiang, Removal of elemental mercury by bamboo charcoal impregnated with H_2O_2, Fuel 90 (2011) 1471–1475.
[21] K. Johari, N. Saman, S.T. Song, C.S. Chin, H. Kong, H. Mat, Adsorption enhancement of elemental mercury by various surface modified coconut husk as eco-friendly low-cost adsorbents, Int. Biodeterior. Biodegrad. 109 (2016) 45–52.
[22] G. Tan, W. Sun, Y. Xu, H. Wang, X. Nan, Sorption of mercury (ii) and atrazine by biochar, modified biochars and biochar based activated carbon in aqueous solution, Bioresour. Technol. 211 (2016) 727–735.
[23] H.C. Hsi, C.Y. Tsai, T.H. Kuo, C.S. Chiang, Development of low-concentration mercury adsorbents from biohydrogen-generation agricultural residues using sulfur impregnation, Bioresour. Technol. 102 (2011) 7470–7477.
[24] M. De, R. Azargohar, A.K. Dalai, S.R. Shewchuk, Mercury removal by bio-char based modified activated carbons, Fuel 103 (2013) 570–578.
[25] G. Li, B. Shen, W. Yi, S. Yue, Y. Xi, M. An, K. Ren, Comparative study of element mercury removal by three bio-chars from various solid wastes, Fuel 145 (2015) 189–195.
[26] Z. Tan, L. Sun, J. Xiang, H. Zeng, Z. Liu, S. Hu, J. Qiu, Gas-phase elemental mercury removal by novel carbon-based sorbents, Carbon 50 (2012) 362–371.
[27] Z. Tan, G. Niu, X. Chen, Removal of elemental mercury by modified bamboo carbon, Chin. J. Chem. Eng. 23 (2015) 1875–1880.
[28] R.K. Gupta, M. Dubey, P. Kharel, Z. Gu, Q.H. Fan, Biochar activated by oxygen plasma for supercapacitors, J. Power Sources 274 (2015) 1300–1305.
[29] P.S.D.V. Maldonado, V. Hernández-Montoya, A. Concheso, M.A. Montes-Morán, Formation of cerussite and hydrocerussite during adsorption of lead from aqueous solution on oxidized carbons by cold oxygen plasma, Appl. Surf. Sci. 386 (2016) 381–388.
[30] P.S.D.V. Maldonado, V. Hernández-Montoya, M.A. Montes-Morán, Plasma-surface modification vs air oxidation on carbon obtained from peach stone: textural and chemical changes and the efficiency as adsorbents, Appl. Surf. Sci. 384 (2016) 143–151.
[31] W.W. Su, W. Wang, Y.L. Li, L. Xu, R. Wang, Fabrication of antimony-doped tin oxide/carbon black composite with oxygen plasma treatment for lithium-air batteries, Mater. Lett. 180 (2016) 203–206.
[32] B. Zhang, P. Xu, Y. Qiu, Q. Yu, J. Ma, H. Wu, G. Luo, M. Xu, H. Yao, Increasing oxygen functional groups of activated carbon with non-thermal plasma to enhance mercury removal efficiency for flue gases, Chem. Eng. J. 263 (2015) 1–8.
[33] B. Zhang, X. Zeng, P. Xu, J. Chen, Y. Xu, G. Luo, M. Xu, H. Yao, Using the novel method of non-thermal plasma to add Cl active sites on activated carbon for mercury removal in flue gas, Environ. Sci. Technol. 50 (2016) 11837–11843.
[34] J. Zhang, Y. Duan, Q. Zhou, C. Zhu, M. She, W. Ding, Adsorptive removal of gas-phase mercury by oxygen non-thermal plasma modified activated carbon, Chem. Eng. J. 294 (2016) 281–289.
[35] Y. Gu, Y. Zhang, L. Lin, H. Xu, W. Orndorff, W.P. Pan, Evaluation of elemental mercury adsorption by fly ash modified with ammonium bromide, J. Therm. Anal. Calorim. 119 (2015) 1663–1672.
[36] J. Wang, Y. Zhang, L. Han, L. Chang, W. Bao, Simultaneous removal of hydrogen sulfide and mercury from simulated syngas by iron-based sorbents, Fuel 103 (2013) 73–79.
[37] D. Hauchecorne, B.J.V.D. Veken, A. Moiana, W.A. Herrebout, The C–Cl···N halogen bond, the weaker relative of the C–I and C–Br···N halogen bonds, finally characterized in solution, Chem. Phys. 374 (2010) 30–36.
[38] V.T. Santana, S.P.C. Gonçalves, J.A.M. Agnelli, S.M. Martins-Franchetti, Biodegradation of a polylactic acid/polyvinyl chloride blend in soil, J. Appl. Polym. Sci. 125 (2012) 536–540.
[39] G. Lota, J. Tyczkowski, R. Kapica, K. Lota, E. Frackowiak, Carbon materials modified by plasma treatment as electrodes for supercapacitors, J. Power Sources 195 (2010) 7535–7539.
[40] G. Li, B. Shen, L. Feng, The mechanism of sulfur component in pyrolyzed char from waste tire on the elemental mercury removal, Chem. Eng. J. 273 (2015) 446–454.
[41] I. Diamantopoulou, G. Skodras, G.P. Sakellaropoulos, Sorption of mercury by activated carbon in the presence of flue gas components, Fuel Process. Technol. 91 (2010) 158–163.
[42] H. Zeng, J. Feng, J. Guo, Removal of elemental mercury from coal combustion flue gas by chloride-impregnated activated carbon, Fuel 83 (2004) 143–146.
[43] S.J. Lee, Y.C. Seo, J. Jurng, G.L. Tai, Removal of gas-phase elemental mercury by iodine- and chlorine-impregnated activated carbons, Atmos. Environ. 38 (2004) 4887–4893.
[44] S. Tao, C. Li, X. Fan, G. Zeng, P. Lu, X. Zhang, Q. Wen, W. Zhao, D. Luo, C. Fan, Activated coke impregnated with cerium chloride used for elemental mercury removal from simulated flue gas, Chem. Eng. J. 210 (2012) 547–556.
[45] Y. Xu, X. Zeng, G. Luo, B. Zhang, P. Xu, M. Xu, H. Yao, Chlorine-char composite synthesized by co-pyrolysis of biomass wastes and polyvinyl chloride for elemental mercury removal, Fuel 183 (2016) 73–79.